Analytical Biochemistry **301,** 261–277 (2002)
doi:10.1006/abio.2001.5503, available online at http://www.idealibrary.com on IDEAL®

Radiative Decay Engineering

2. Effects of Silver Island Films on Fluorescence Intensity, Lifetimes, and Resonance Energy Transfer

Joseph R. Lakowicz, Yibing Shen, Sabato D'Auria, Joanna Malicka, Jiyu Fang,* Zygmunt Gryczynski, and Ignacy Gryczynski

*Center for Fluorescence Spectroscopy, Department of Biochemistry and Molecular Biology, University of Maryland Baltimore, 725 West Lombard Street, Baltimore, Maryland 21201; and *Center for Biomolecular Science and Engineering, NRL, Washington, DC 20375*

Received July 16, 2001; published online January 15, 2002

Metallic surfaces can have unusual effects on fluorophores such as increasing or decreasing the rates of radiative decay and the rates of resonance energy transfer (RET). In the present article we describe the effects of metallic silver island films on the emission spectra, lifetimes, and energy transfer for several fluorophores. The fluorophores are not covalently coupled to the silver islands so that there are a range of fluorophore-to-metal distances. We show that proximity of fluorophores to the silver islands results in increased fluorescence intensity, with the largest enhancement for the lowest-quantum-yield fluorophores. Importantly, the metal-induced increases in intensity are accompanied by decreased lifetimes and increased photostability. These effects demonstrate that the silver islands have increased the radiative decay rates of the fluorophore. For solvent-sensitive fluorophores the emission spectra shifted to shorted wavelengths in the presence of the silver islands, which is consistent with a decrease of the apparent lifetime for fluorophores near the metal islands. We also observed an increased intensity and blue spectral shift for the protein human glyoxalase, which displays a low quantum yield for its intrinsic tryptophan emission. In this case the blue shift is thought to be due to increased emission from a buried low-quantum-yield tryptophan residue. Increased intensities were also observed for the intrinsic emission of the nucleic acid bases adenine and thymine and for single-stranded 15-mers poly(T) and poly(C). And finally, we observed increased RET for donors and acceptors in solution and when bound to double-helical DNA. These results demonstrate that metallic particles can be used to modify the emission from intrinsic and extrinsic fluorophores in biochemical systems.

Fluorescence experiments are typically performed in sample geometries that are large relative to the size of the fluorophores and relative to the absorption and emission wavelengths. In this arrangement the fluorophores radiate into free space. Most of our knowledge and intuition about fluorescence is derived from the spectral properties observed in these free-space conditions. However, the presence of nearby metallic surfaces or particles can alter the free-space condition, which can result in dramatic spectral changes which are distinct from those observable in the absence of metal surfaces. For clarity we note that "metal" refers to a highly conducting particle or surface, and not metal ions or oxides. Remarkably, metal surfaces can increase or decrease the radiative decay rates of fluorophores and increase the extent of resonance energy transfer (RET).[1] These effects are due to interactions of the excited-state fluorophores with free electrons in the metal, which polarize the metal and impose a reactive field on the fluorophore. These effects have been the subject of many publications (1–6). The effects of metallic surfaces are complex and include quenching at short distances, spatial variation of the incident light field, and changes in the radiative decay rates. It has also been predicted that metallic particles can increase the rate of energy transfer (7, 8). Different effects are

[1] Abbreviations used: AFM, atomic force microscopy; AO, acridine orange; BF, basic fucsin; bpy, 2,2′-bipyridine; CT, calf thymus; DAPI, 4′,6-diamidino-2-phenylindole; dppz, dipyrido[3,2-*a*:2′,3′-*c*]phenazine; DMF, dimethylformamide; DODCI, 3,3′-diethyloxadicarbocyanine iodide; ErB, erythrosin B; phen, 9,10-phenanthroline; prodan, 6-propionyl-2-(dimethylamino)naphthalene; Py2, pyridine 2; R6G, rhodamine 6G; RhB, rhodamine B; RB, rose bengal; RET, resonance energy transfer; SERS, surface-enhanced Raman scattering; SIF, silver island film.

0003-2697/02 $35.00

expected for mirrors, subwavelength or semitransparent metal surfaces, silver island films, and metal colloids.

In our opinion, the effects of metallic surfaces provide a unique opportunity to increase the radiative decay rate of fluorophores. The radiative decay rate of the fluorophore normally is a fundamental property of a fluorophore. This rate is determined by the extinction coefficient (9) and is only weakly dependent on environment. The radiative decay rate varies in proportion to the extinction coefficient (9). In the absence of optical discontinuities the radiative rate and extinction coefficient change by only a few percent between different transparent media. In most fluorescence experiments the spectral changes are due to extrinsic factors that provide additional routes of nonradiative decay, including quenching, RET, and changes in temperature. However, unusual spectral changes are expected for metal-induced changes in the radiative rates. If the radiative rate increases one expects the quantum yield to increase while the lifetime decreases, and vice versa. Increases in the radiative rate can result in useful emission from weakly fluorescent molecules. Some of these predicted effects have been confirmed by experiments (10–12).

In the present article we describe the effects of metal island films on the intensity and intensity decays of fluorophores with various quantum yields and on biochemical fluorophores. Metal island films consist of subwavelength size patches of metal on inert substrates. These particles display surface plasmon absorption, which in the small particle limit can be calculated from the real and imaginary dielectric constants of the metal (13–15). The expected effects of metals on biochemical fluorophores have been summarized in a recent review (16). We now show that proximity to silver islands results in a preferential increase in intensity of low-quantum-yield fluorophores, and that the lifetimes decrease as the intensities increase. In our case the sample is placed between two silver island films. Metal surfaces are shown to result in blue shifts in the emission spectra of solvent-sensitive fluorophores, which we attribute to decreased lifetimes near the metal surfaces. We also show increased apparent Forster distances for donors and acceptors bound to DNA. And finally we show increases in the intrinsic emission of nucleic acid bases and single-stranded DNA. In the Appendix we provide a more quantitative theory and interpretation of the data from our heterogeneous samples. We believe the use of metal surfaces provides numerous opportunities for new methods in fluorescence spectroscopy.

THEORY

The theory for the interaction of fluorophores with metals is complex. An understanding of the physics of these interactions requires solving Maxwell's equations for assumed metallic surfaces and fluorophores (17). We do not consider the underlying physics, but instead focus on the expected spectral changes. In the absence of external quenching processes the lifetime (τ_0) and quantum yield (Q_0) of a fluorophore are determined by the rate of radiative decays (Γ) and the rate of nonradiative decay to the ground state (k_{nr}). The quantum yield is given by

$$Q_0 = \Gamma/(\Gamma + k_{nr}). \quad [1]$$

The observed lifetime in the absence of other quenching interactions is given by

$$\tau_0 = (\Gamma + k_{nr})^{-1}. \quad [2]$$

The natural lifetime of a fluorophore (τ_N) is the inverse of the radiative decay rate ($\tau_N = \Gamma^{-1}$), which is the lifetime if $k_{nr} = 0$ or $Q = 1.0$. The natural lifetime as well as the extinction coefficient of a fluorophore is determined by the oscillator strength of the electronic transition (9) and by the photonic mode density (3). In a continuous transparent medium the photonic mode density is spatially invariant and is completely defined by the refractive index of the medium, which results in a well-known expression for the natural lifetime (9).

The measured lifetime of a fluorophore can be increased or decreased by changing the value of k_{nr}. Suppose the fluorophore is exposed to a collisional quencher or other nonradiative process with a rate $k_q[Qu]$ which competes with emission, where [Qu] is the concentration of quencher and k_q is the biomolecular quenching constant. In this case the quantum yield (Q) and lifetime (τ) are given by

$$Q = \Gamma/(\Gamma + k_{nr} + k_q[Qu]), \quad [3]$$

$$\tau = (\Gamma + k_{nr} + k_q[Qu])^{-1}. \quad [4]$$

These expressions show that the quantum yield and lifetimes of the quenched (Eqs. [3] and [4]) or unquenched (Eqs. [1] and [2]) fluorophore increase or decrease together with changes in quenching or the nonradiative decay rates.

The presence of a nearby metallic surface can modify the radiative rate of an excited fluorophore. Suppose a fluorophore is located at a given distance from a metallic surface and that the radiative rate increases and is given by Γ_m. The quantum yield (Q_m) and lifetime (τ_m) of the fluorophore are now given by

$$Q_m = \frac{\Gamma + \Gamma_m}{\Gamma + \Gamma_m + k_{nr}}, \quad [5]$$

$$\tau_m = (\Gamma + \Gamma_m + k_{nr})^{-1}. \quad [6]$$

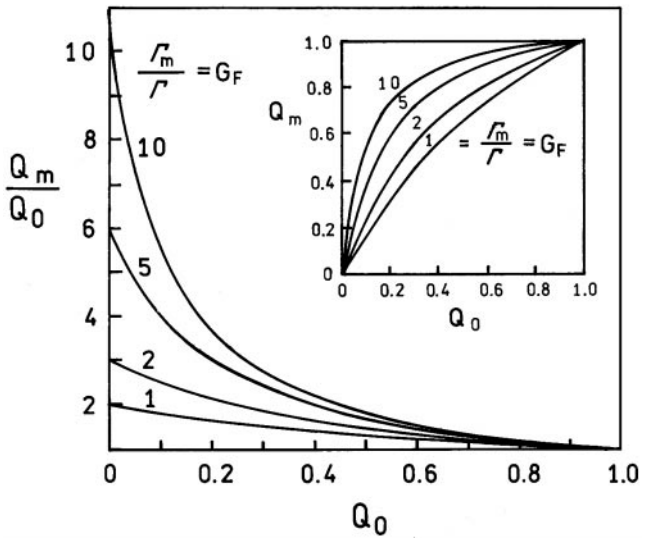

FIG. 1. Effect of metal-induced increase in Γ_m on the yield enhancement (Q_m/Q_0) and quantum yield of fluorophores in the presence of a metal (Q_m) with various quantum yields (Q_0).

In principle Γ_m can take on values from $-\Gamma$ to ∞. Suppose a fluorophore displays a low quantum yield, which implies $k_{nr} \gg \Gamma$. As the value of Γ_m increases, the lifetime decreases. However, in contrast to collisional quenching (Eqs. [3] and [4]), the quantum yield increases. Examination of Eq. [5] suggests that high quantum yields can be obtained whenever Γ_m is comparable to k_{nr}.

It is informative to consider the effects of increases in the value of Γ_m for fluorophores with different quantum yields. Figure 1 shows the expected enhancements (Q_m/Q_0) and quantum yields (Q_m) for a fluorophore in a homogeneous environment for various values of Γ_m. As Γ_m becomes larger than Γ the emission of the fluorophore is increased ($Q_m/Q_0 > 1$), and the quantum yield increases. Importantly, these effects are larger for fluorophores with lower quantum yields. A quantum yield of unity cannot be increased by an increase in Γ_m. However, the lifetime can be decreased (Eq. [6]).

Relative Intensities with and without SIFs

In this article we report values of the fluorescence intensity between quartz plates in the absence of SIFs (I_Q) and between silver island films (I_S). The experimental geometry is shown in Scheme 1. The sample consists of two quartz plates, which may be uncoated (one part of sample) or coated with SIFs. The sample is about 1 μm thick. Most of the sample is distant from the SIFs and displays an unperturbed quantum yield Q_0 and a lifetime τ_0. Some of the sample is in close proximity to the SIFs and is quenched, $Q_q = 0$. For our purposes the important part of the sample is in the enhanced region of thickness d_m with a quantum yield Q_m and a lifetime τ_m. In this region we assume the radiative rate is increased by a factor G_F and is given by $\Gamma_m = G_F\Gamma$. It is also possible that the absorption in this region is increased by a factor G_A, yielding an effective extinction coefficient $\epsilon_m = G_A\epsilon_0$, where ϵ_0 is the free-space, extinction coefficient. As shown in the Appendix the ratio of intensities between the SIFs (S) to that between the quartz (Q) plates is given by

$$\frac{I_S}{I_Q} = \frac{d - 2(d_m + d_q)}{d} + \frac{2G_A d_m}{d}\frac{G_F(\Gamma + k_{nr})}{G_F\Gamma + k_{nr}}. \quad [7]$$

One can see that the ratio of observed intensities depends on the thickness of the enhanced volume, the enhancement of absorption and emission, and the relative quantum yield:

$$\frac{Q_m}{Q_0} = \frac{G_F(\Gamma + k_{nr})}{G_F\Gamma + k_{nr}}. \quad [8]$$

We consider two limiting cases, the first where both the absorption and emission are equally enhanced ($G_F = G_A = G$), and the second where only the emission is affected by the SIFs ($G_A = 1.0$). At present it is not possible to recover all the parameters in eq. [7]. Instead we make reasonable assumptions to estimate the values of G and d_m.

MATERIALS AND METHODS

Procedure for Making Silver Nanoparticle Films

The chemicals used to generate silver particles, silver nitrate (99+%), sodium hydroxide (pellets, 97%), ammonium hydroxide (NH_3 content 28–30%), and D-glucose (99.5%) were purchased from Aldrich/Sigma and used without further purification. All procedures were performed using distilled water which was fur-

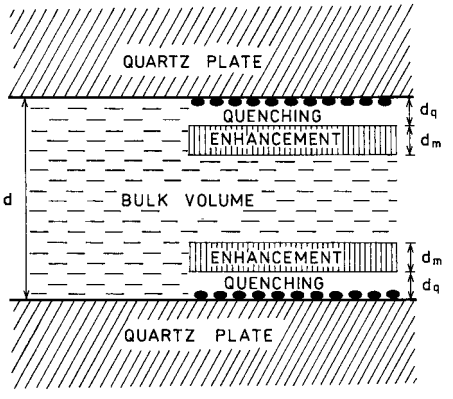

SCHEME 1. Schematic for a fluorophore solution between two silver island films. The solid ellipsoids represent the silver island films.

ther purified by Millipore filtration. Silver islands were formed on quartz microscope slides. The use of quartz provided UV transmission and less autofluorescence. The quartz slides used to deposit silver particles were soaked in a 10:1 (v/v) mixture of H_2SO_4 (95–98%) and H_2O_2 (30%) overnight before the deposition. They were washed with water and air-dried prior to use.

Silver deposition was carried out in a clean 30-ml beaker equipped with a Teflon-coated stir bar. To a fast stirring silver nitrate solution (0.22 g in 26 ml of Millipore water), 8 drops of fresh 5% NaOH solution were added. Dark-brownish precipitates formed immediately. Less than 1 ml of ammonium hydroxide was then added drop by drop to redissolve the precipitates. The clear solution was cooled to 5°C by placing the beaker in an ice bath, followed by soaking the cleaned and dried quartz slides in the solution. At 5°C, a fresh solution of D-glucose (0.35 g in 4 ml of water) was added. The mixture was stirred for 2 min at that temperature. Subsequently, the beaker was removed from the ice bath. The temperature of the mixture was allowed to warm up to 30°C. As the color of the mixture turning from yellow green to yellowish brown, the color of the slides become greenish; the slides were removed and washed with water and bath sonicated for 1 min at room temperature. After being rinsed with water several times, the slides were stored in water for several hours prior to the experiments. Atomic force microscopy (AFM) studies of nanoparticles were carried out using a Nanoscope IIIa (Digital Instruments). All the images were taken with noncontact silicon nitride probes (NCL-16) manufactured by Nanosensors. The cantilevers with these probes have a resonance frequency of approximately 170 kHz and a nominal spring constant of approximately 40 N/m. Image analysis was carried out using the Digital Instrument Image processing software. Scheme 2 shows an AFM image of the SIFs. The size of most silver particles is between 300 and 400 Å. Aggregate particles are also present.

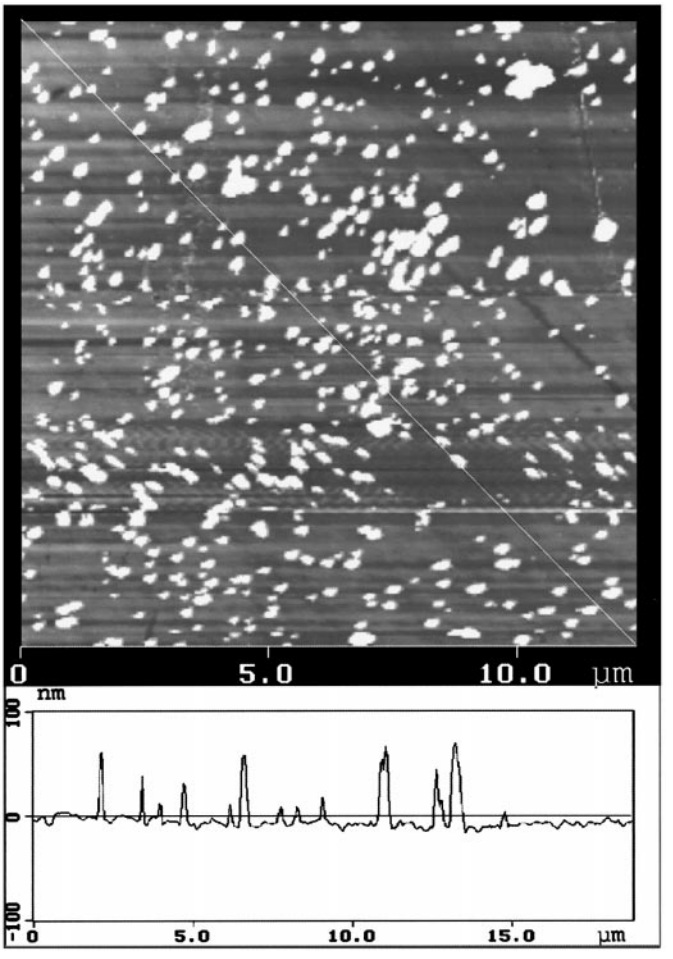

SCHEME 2. Atomic force microscope image of the silver island film on quartz.

Experimental Procedures

The protein *E. coli* β-galactosidase was obtained by Sigma and human glyoxalase was obtained using known procedures (18–20). The proteins were dissolved in 10 mM phosphate buffer, pH 6.5. The concentrations of β-galactosidase and human glyoxalase were 0.05 and 0.15 mg/ml, respectively. For these studies of intrinsic protein fluorescence the excitation wavelength was 295 nm. Adenine, thymine, and calf thymus DNA were obtained from Sigma. Poly(T) and poly(C), each 15 bases long, were obtained from the Biopolymer Core facility at the University of Maryland School of Medicine, and were dissolved in 10 mM phosphate buffer, pH 7.0.

Emission spectra were obtained using a SLM 8000 spectrofluorometer. Intensity decays were measured in the frequency domain using instrumentation described previously (20, 21). For rhodamine B (RhB) and rose bengal (RB) the excitation was at 514 nm from the approximate 78-MHz output of a mode-locked argon ion laser. For the frequency-domain measurements the emission was observed through a combination of a glass cutoff filter (Corning 3-69) and a 580-nm interference filter. For all steady-state and frequency-domain measurements the excitation was vertically polarized and the emission observed through a horizontally oriented polarizer to minimize scattered light. The frequency-domain intensity decay data were analyzed in terms of the multiexponential model

$$I(t) = \sum_i \alpha_i \exp(-t/\tau_i), \qquad [9]$$

where τ_i are the lifetimes with amplitudes α_i and $\Sigma \alpha_i = 1.0$. Fitting to the multiexponential model was

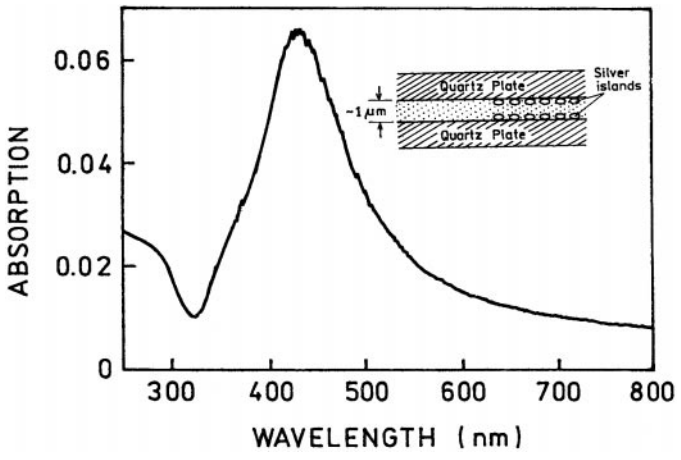

FIG. 2. Absorption spectrum of silver islands deposited on a quartz plate.

performed as described previously (22). The contribution of each component to the steady-state intensity is given by

$$f_i = \frac{\alpha_i \tau_i}{\sum_j \alpha_j \tau_j}. \qquad [10]$$

The mean lifetime is given by

$$\bar{\tau} = \sum f_i \tau_i, \qquad [11]$$

where $\Sigma f_i = 1.0$.

RESULTS

Silver Island Films and Experimental Geometry

Figure 2 shows the absorption spectra of our silver island films. This spectrum indicates that the particles are subwavelength in size. In the small-particle limit the absorption maximum due to this plasmon resonance is expected to be near 380 nm (23, 24). Our absorption maximum above 400 nm can be due to an asymmetric effective shape of the particles with an axial ratio near 1.5 to 1.0 (23) and is also consistent with silver particles with spherical dimensions near 40–50 nm (25–27). The shape and size distribution of the particles is almost certainly heterogeneous.

To determine the effects of silver islands on fluorescence the samples were placed between two such silver island plates. From the absorption spectra of rose bengal between two quartz plates or two silver island-coated plates (Fig. 3) we estimate the distance between the plates to be 1 to 1.5 μm.

Effects of Silver Island Films on Emission Spectra of Rhodamine B and Rose Bengal

As an initial experiment we examined the emission spectra of rhodamine B (RhB) and rose bengal (RB) between uncoated quartz plates (Q) or silver island films (S). We selected these two fluorophores because of their similar absorption and emission spectra but different quantum yields of 0.48 and 0.02 for RhB and RB, respectively. In the case of RhB the intensities are similar in the absence and presence of these silver islands (Fig. 4, top). There may be a small increase in the RhB intensity due to the silver islands. Since the quantum yield of RhB is high, it cannot be substantially increased by the silver islands.

It is of interest to consider the magnitude of the metal-induced spectral changes which could account for the approximate 20% increase in intensity seen for RhB between SIFs. Suppose the quenching and enhancement values had a thickness $d_q = d_m = 100$ Å, and the total sample thickness $d = 10{,}000$ Å. Assume further that the SIFs increase both the absorption and radiative rate by 20-fold. Then using Eqs. [7] and [8], and the data in Table 3 (below), the expected value of I_S/I_Q is 1.34. This value is reasonably close to the measured value of I_S/I_Q, 1.20. We note that we are not attempting to fit the data to Eq. [7], but rather are asking what range of effects on Γ and ϵ_0 are consistent with the observation.

Contrasting results were obtained for rose bengal (Fig. 4, bottom). In this case the intensity increased

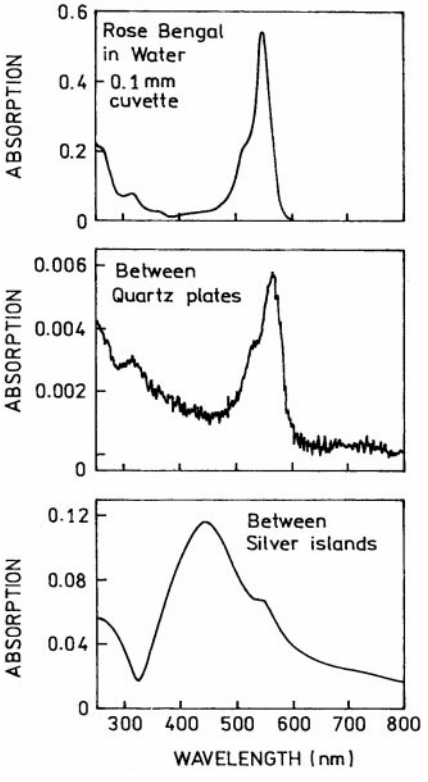

FIG. 3. Absorption spectra of rose bengal in a 0.1-mm cuvette (top), between quartz plates (middle), and between quartz slides coated with silver islands (bottom).

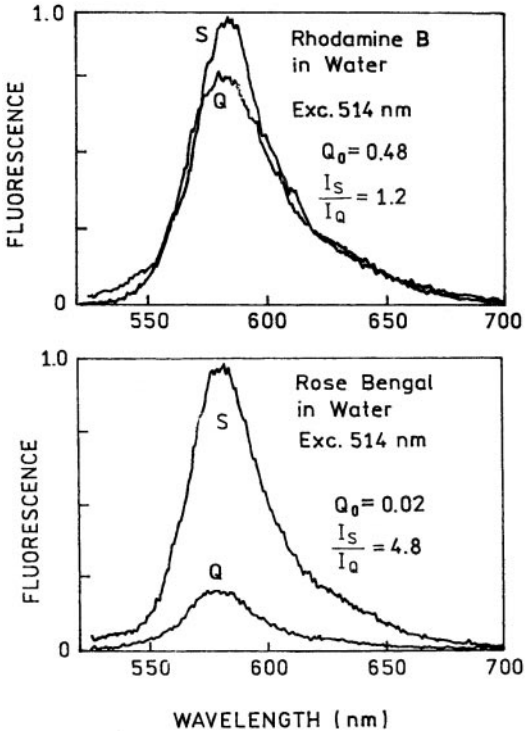

FIG. 4. Emission spectra of rhodamine B (top) and rose bengal (bottom) between silver island films (S) or unsilvered quartz plates (Q).

about five-fold in the presence of silver islands. It is important to recognize that the increased intensity observed for RB represents an underestimation of the quantum yield of RB near the silver islands. This is because only a small fraction of the RB molecules are within the distance over which metallic surfaces can exert effects. The region of varying photonic mode density is expected to extend about λ/4 or 200 Å into the solution. Hence only about 4% of the liquid volume between the plates is within the active volume. This suggests that the quantum yield of RB within 200 Å of the islands is increased 125-fold. Of course this is larger than possible if the quantum yield of 0.02 is correct. Nonetheless, the spectrum for RB in Fig. 4 indicates a substantial increase in quantum yield for the molecule within 200 Å of the silver islands. We calculated the expected intensity ratio for RB using the same parameter values used for RhB. This calculation predicts a ratio of 2.8, which is roughly comparable to the measured ratio.

We questioned how the effects seen in Fig. 4 depended on the density of the silver island films. We examined the enhancement for RhB (Fig. 5) and rose bengal (Fig. 6) as the amount of deposited silver increased. This was accomplished by allowing the cleaned quartz slides to remain in the silver deposition solution for various amounts of time ranging from 6 to 15 min. As the deposition time increases, the plasmon absorption increases and the absorption maximum shifts to longer wavelengths. For RhB the emission intensity was not affected by the deposition time (Fig. 5). For rose bengal progressively larger enhancements were found for larger amounts of deposited silver (Figs. 6 and 7). We attempted to examine these effects of still higher densities of silver on the quartz slides. However, the emission spectra of RhB and rose bengal were distorted for higher plasmon absorption (not shown).

Effect of Silver Island Films on Photostability

The photostability of fluorophores is an important property in fluorescence microscopy and in single-molecule detection (28–30). It is known that this extent of fluorophore photodecomposition is roughly proportional to the time a fluorophore remains in the excited state, as has been shown by increased donor photostability in the presence of a RET acceptor (31). This suggests that the increased radiative decay rates of fluorophores near metal islands or colloids could result in increased photostability and easier single-molecule detection.

We examined the effects of silver island films on the photostability of RhB and rose bengal. For RhB the rate of photobleaching was unchanged by the silver island films (Fig. 8, right), which is consistent with most of the emission being due to RhB molecules dis-

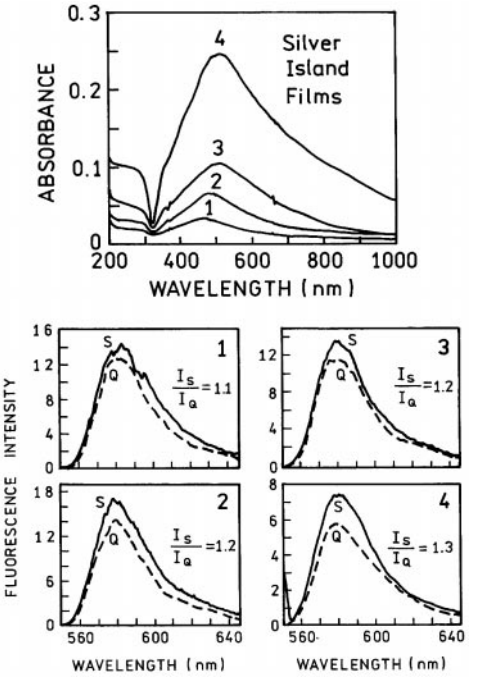

FIG. 5. Dependence of rhodamine B fluorescence on silver island film preparation. The emission spectra near silver islands (S) correspond to the numbered absorption spectra (top).

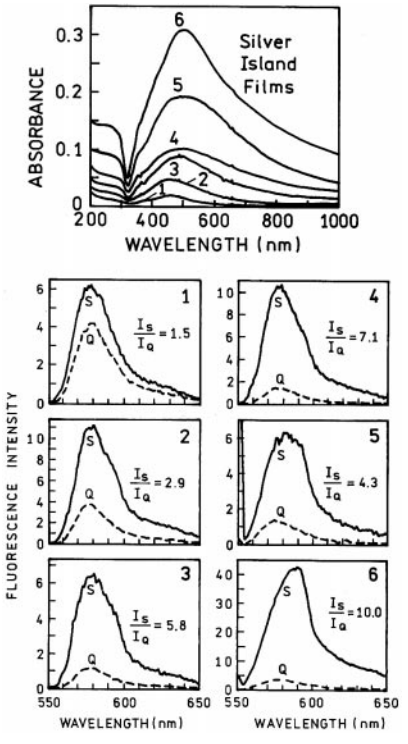

FIG. 6. Dependence of rose bengal fluorescence on silver island film preparation. The emission spectra near silver islands (S) correspond to the numbered absorption spectra (top).

tant from the metal island films. For rose bengal there was a dramatic increase in photostability in the presence of the silver island films (Fig. 8, left). This result is consistent with an increase in the radiative decay rate of rose bengal in the fraction of molecules close to the films, and also with the decreased lifetimes (below). These results indicate that the increased intensity seen for rose bengal (Figs. 4 and 6) is not due to an

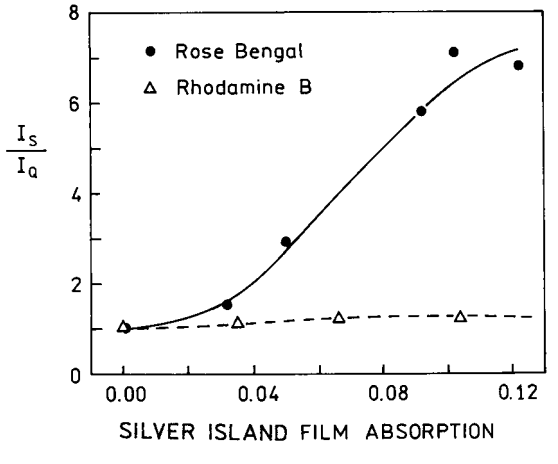

FIG. 7. Dependence of fluorescence enhancement on silver island film absorption.

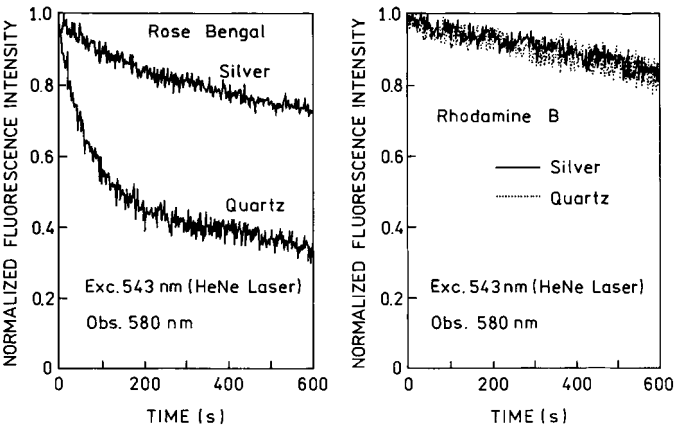

FIG. 8. Photostability of rose bengal and rhodamine B aqueous solutions on quartz and on silver island films. The excitation source was a 543-nm HeNe laser (Melles Griot, 0.8 mW) focused into a 0.5-mm spot.

increased local field or rate of excitation because such effects would increase the rate of photobleaching or leave the rate unchanged. These results suggest that fluorophores on metal colloids may provide photostable probes for microscopy, and that the number of photons detectable from a single fluorophore can be increased near metallic particles.

Under the conditions used for Fig. 8 we did not detect a difference in the photobleaching of RhB between

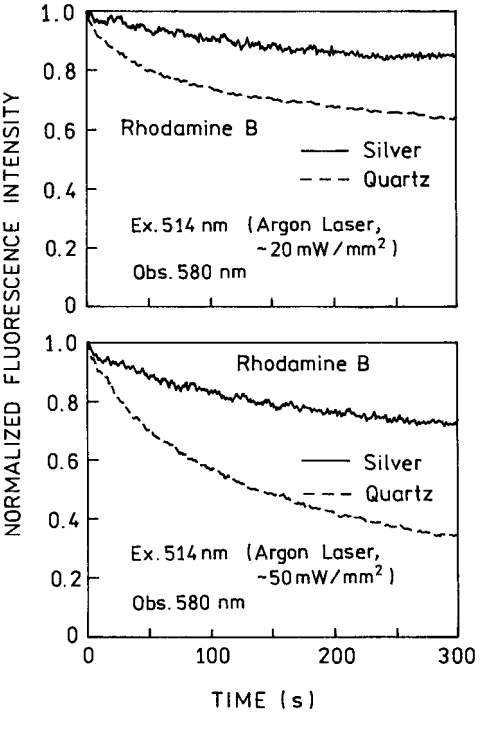

FIG. 9. Photostability of rhodamine B in water between quartz plates (- - -) and between SIFs (—). The excitation source was a Coherent argon Ion laser at 514 nm.

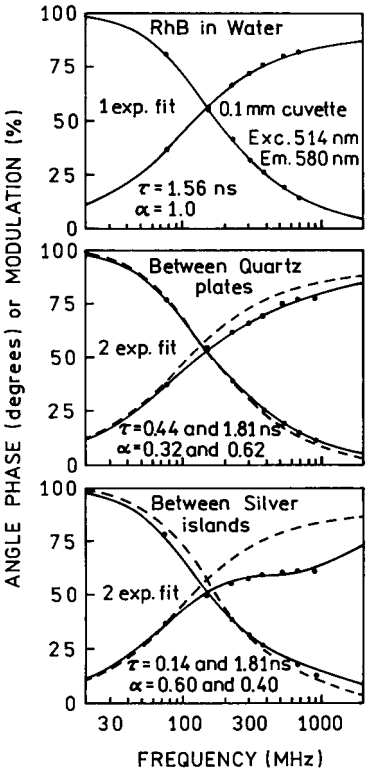

FIG. 10. Frequency-domain intensity decays of rhodamine B in water when placed in a 0.1-mm cuvette (top), between quartz plates (middle), and between silver islands (bottom). In the lower two panels the dashed lines represent the FD data for RhB in the 0.1-mm cuvette (from the top panel).

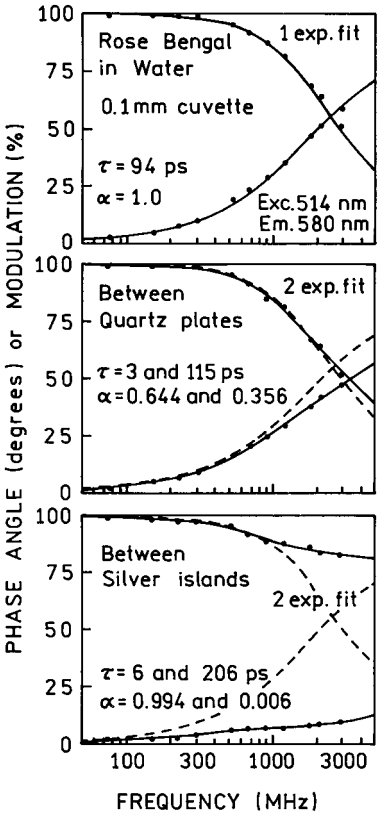

FIG. 11. Frequency-domain intensity decays of rose bengal in water when placed in 0.1-mm cuvette (top), between quartz plates (middle), and between silver islands (bottom). In the lower two panels the dashed lines represent the FD data for rose bengal in the 0.1-mm cuvette (from the top panel).

quartz plates or between SIFs. Hence we increased the illumination intensity using the 514-nm output of an argon ion laser. Under these conditions we observed RhB photobleaching and increased photostability of RhB between the SIFs (Fig. 9). The difference between quartz and SIFs increased as the incident intensity increased. The emission spectra were essentially unchanged at the end of the 300-s photobleaching runs. We interpret these results as due to photobleaching of the RhB distant from the silver islands, and the remaining signal as due to more photostable RhB molecules close to the silver islands. As shown below, the intensity decay data support this interpretation.

Effects of Silver Island Films on the Lifetime of RhB and Rose Bengal

The effects of an increased radiative rate and concentrated electric field can be distinguished by lifetime

TABLE 1

Multiexponential Intensity Decay of Rhodamine B and Rose Bengal Intensity Decays

Fluorophore	$\bar{\tau}$ (ns)[a]	τ_1 (ns)	τ_2 (ns)	α_1	α_2	f_1	f_2	χ^2_R
Rhodamine B								
0.1-mm cuvette	1.57	1.57	—	1.0	—	1.0	0	1.7
Quartz plates	1.67	0.44	1.81	0.318	0.682	0.102	0.898	2.9
Silver islands	1.63	0.14	1.81	0.597	0.403	0.105	0.895	3.8
Rose bengal								
0.1-mm cuvette	0.094	0.094	—	1.0	—	1.0	0	2.6
Quartz plates	0.079	0.003	0.115	0.644	0.356	0.321	0.679	1.9
Silver islands	0.039	0.006	0.206	0.994	0.006	0.831	0.169	1.2

[a] $\bar{\tau} = \Sigma f_i \tau_i$ (Eq. [11]).

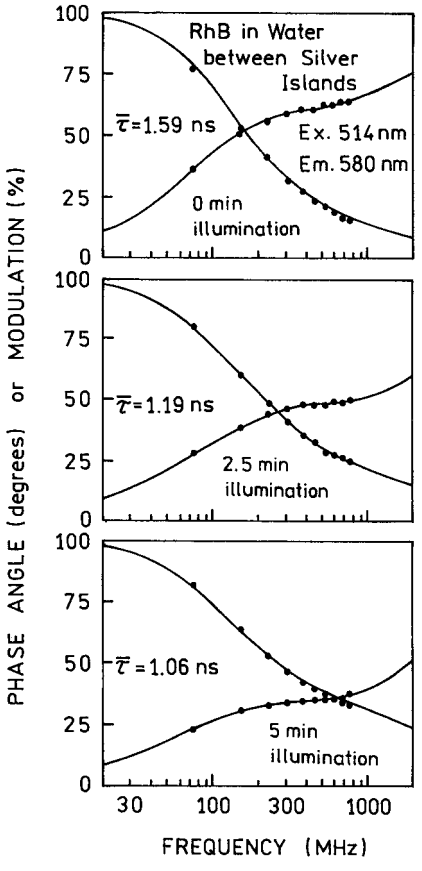

FIG. 12. Frequency-domain intensity decays of RhB between SIFs during photobleach at 514 nm.

measurements. An increase in the radiative rate will decrease the lifetime (Eq. [6]) whereas an increased rate of excitation will not change the lifetime. We measured the intensity decays of RhB and rose bengal in the absence and presence of silver islands. In a standard cuvette the intensity decay of RhB was found to be a single exponential with a lifetime $\tau = 1.56$ ns (Fig. 10). In the presence of silver islands the intensity decay becomes heterogeneous. The data could be fit to two decay times (Table 1), with the long lifetime of 1.81 ns being comparable to that found in a cuvette. A short lifetime of 0.14 ns appeared for RhB between the silver islands which we attribute to RhB molecules in close proximity to the silver islands. The fractional steady-state intensity of this short component is about 10%. Control measurements showed that this component was not due to scattered light. Measurements were also performed for RhB between quartz plates without silver islands. In this case the decay was also double exponential, but less heterogeneous than in the presence of islands. Nonetheless it is clear that a short-lifetime component appears for RhB between silver islands. Control measurements showed there was no significant intensity for the quartz slides alone without RhB. This result suggests that scattered light is not the origin of the short component seen for RhB between uncoated slides. At present we do not understand the origin of the 0.44-ns component for RhB between uncoated quartz plates.

Frequency-domain intensity decays for rose bengal are shown in Fig. 11. In a cuvette the decay is a single exponential with $\tau = 94$ ps. The decay become slightly heterogeneous for rose bengal between uncoated quartz plates. However, the intensity decay of rose bengal changed dramatically when between silver islands. In this case the dominant lifetime became a 6-ps component, which we assign to rose bengal molecules adjacent to the silver islands. This dramatic decrease in the lifetime of rose bengal is consistent with the increased photostability seen near the silver islands (Fig. 8).

The photobleaching results suggested that the fluorophores in the bulk solution were being destroyed while those near the silver islands were more photostable. If this is true then one expects a progressive increase in the fractional intensity of the short-lived component as the sample is illuminated. Hence we measured the frequency domain intensity decays dur-

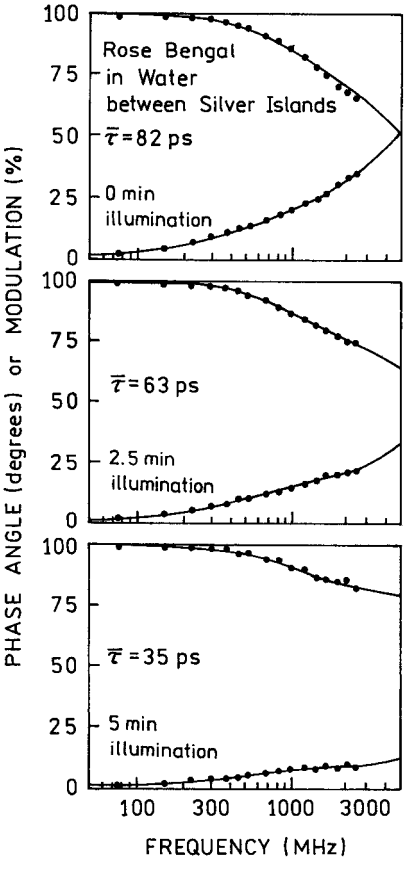

FIG. 13. Frequency-domain intensity decays of RB between SIFs during photobleaching at 514 nm.

TABLE 2

Multiexponential Intensity Decay of Rhodamine B and Rose Bengal between Silver Islands When Illuminated with 514 nm, 50 mW from Argon Ion Laser

Illumination	$\bar{\tau}$ (ns)[a]	τ_1 (ns)	τ_2 (ns)	α_1	α_2	f_1	f_2	χ^2_R
Rhodamine B								
0 min	1.59	0.16	1.74	0.543	0.457	0.100	0.900	1.7
2.5 min	1.19	0.13	1.47	0.751	0.249	0.206	0.794	4.3
5 min	1.06	0.10	1.54	0.884	0.116	0.332	0.668	3.6
Rose bengal								
0 min	0.082	0.035	0.19	0.924	0.076	0.693	0.307	1.6
2.5 min	0.063	0.018	0.17	0.957	0.043	0.707	0.293	1.1
5 min	0.035	0.006	0.16	0.990	0.010	0.805	0.195	1.0

[a] $\bar{\tau} = \sum f_i \tau_i$.

ing photobleaching. For both RhB (Fig. 12) and RB (Fig. 13) we see a progressive shift to higher frequencies during photobleaching. The multiexponential analyses are summarized in Table 2. For RhB, illumination with 50 mM at 514 nm resulted in a progressive increase in the component near 0.15 ns. For RB, illumination resulted in a progressive increase in a component with a decay time near 20 ps. These results support our claim for a short-lifetime photostable component near the silver islands.

It is of interest to consider the observed short lifetime values and expected values for an assumed enhancement factor G_F. Using the parameter values in Table 3 for rose bengal (below) one can calculate a 20-fold increase in Γ results in a decay time of 0.16 ns, in good agreement with the observed short component (Table 2). However, a 20-fold increase in Γ for RB results in a predicted lifetime of 65 ps, considerably longer than the observed values from 6 to 35 ps. We suspect the difference lies in the lower quantum yield of RB as compared with RhB, and this selective observation of the RB molecules closest to the silver islands.

Effect of Quantum Yield on Silver Island Enhancements

The results from RhB and rose bengal were consistent with our expectations. Nonetheless, we were concerned with possible artifacts due to dye binding to the surfaces or other unknown effects. For this reason we examined a number of additional fluorophores between uncoated quartz plates and between silver island films. Emission spectra of four fluorophores are shown in Fig. 14. In all cases the emission was more intense for the solution between the silver islands. For example, $[Ru(bpy)_3]^{2+}$ and $[Ru(phen)_2dppz]^{2+}$ have quantum yields near 0.02 and <0.001, respectively (32–35). A larger enhancement was found for $[Ru(phen)_2dppz]^{2+}$ than for $[Ru(bpy)_3]^{2+}$ (Fig. 14). The enhancements for 10 different fluorophore solutions are shown in Fig. 15. In all cases lower bulk-phase quantum yields result in larger enhancements for samples between silver island films. Additionally, we examined $[Ru(phen)_2dppz]^{2+}$ in water–dimethylformamide (DMF) mixtures (Fig. 16). This compound is quenched by water and the largest

TABLE 3

Photophysical Parameters for the Fluorophores in Fig. 15

Fluorophore	Q	τ (ns)	k_{nr} (ns^{-1})	Γ (ns^{-1})	I_S/I_Q (obs)	I_S/I_Q (calc)[b]	I_S/I_Q (calc)[c]	I_S/I_Q (calc)[d]
RhB (1)[a]	0.95	3.04	0.02	0.31	1.1	1.09	1.01	1.47
RhB (2)	0.48	1.58	0.33	0.30	1.24	1.20	1.11	1.89
Rose bengal (3)	0.26	0.97	0.76	0.27	1.7	1.37	1.29	2.51
Rose bengal (4)	0.18	0.86	0.95	0.21	1.9	1.54	1.46	3.03
Erythrosin B (5)	0.035	0.08	12.1	0.44	2.95	3.53	3.49	6.40
$[Ru(bpy)_3]^{2+}$ (6)	0.023	350	0.003	5.7×10^{-5}	4.7	4.62	4.59	7.25
Rose bengal (7)	0.02	0.09	10.9	0.22	4.9	5.06	5.04	7.51
Basic Fuscin (8)	0.018	0.01	98	2	5.1	5.41	5.40	7.69
$[Ru(bpy)_2(dppz)]^{2+}$ (9)	0.009	—	—	—	8.8	8.27	8.28	8.67
$[Ru(bpy)_2(dppz)]^{2+}$ (10)	$\leq$0.001	—	—	—	18.0	18.1	18.1	9.82

[a] Numbers correspond to those in Fig. 15.
[b] Calculated using Eq. [A5] with $G_F = 203$, $G_A = 17$, $d_m = 31$ Å, and $d_q = 40$ Å fixed.
[c] Calculated using $G_F = 199$, $G_A = 1.0$ fixed, $d_m = 31$ Å, and $d_q = 40$ Å fixed.
[d] Calculated using $G_F = 20$ fixed, $G_A = 97$, $d_m = 23$ Å, and $d_q = 40$ Å.

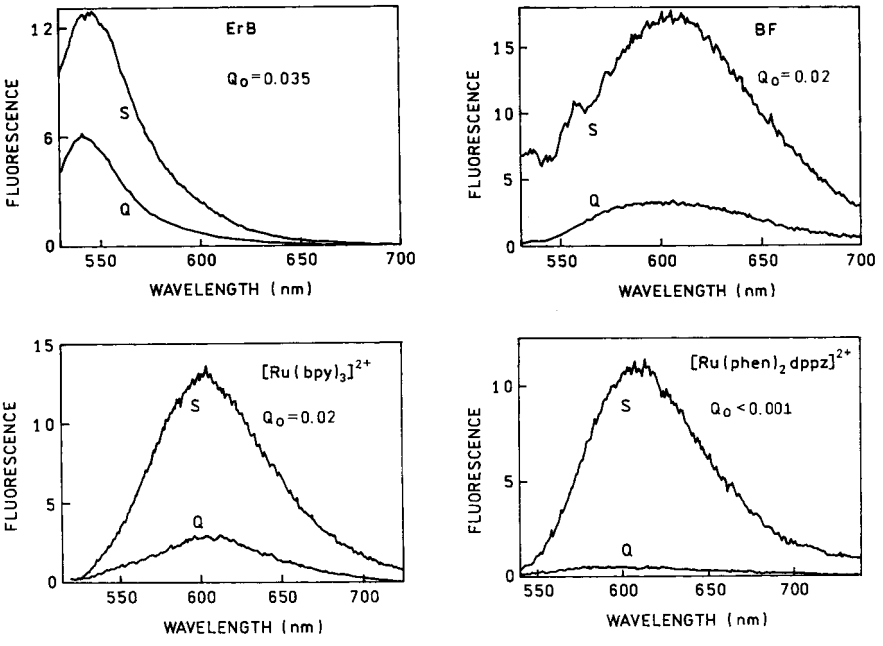

FIG. 14. Emission spectra of fluorophores in aqueous solution between quartz plates (Q) and between two silver island films (S). The quantum yield of $[Ru(bpy)_3]^{2+}$ in air-equilibrated aqueous solution was found to be 0.02, relative to a deoxygenated solution (32, 33).

enhancements were observed for the most-quenched solutions (Fig. 16). Additionally, the dependence of the enhancement (I_S/I_Q) on fluorophore quantum yield roughly followed the simulation shown in Fig. 1. The results in Figs. 14–16 provide strong support for our assertion that proximity of the fluorophore to the metal islands resulted in increased quantum yields. It is unlikely that these diverse fluorophores would all bind to the silver islands or display other unknown effect results that resulted in enhancements that increased monotonically with decreased quantum yields.

In the Appendix we attempt a more quantitative interpretation of the effects seen in Fig. 15. Using this formalism we compared the data in Figs. 15 and 16 with those predicted for various values of G_F, G_A, d_m, and d_q. We found that the data could be explained by values of G_F near 200, but not by smaller values of $G_F = 20$. The larger value of G_F is more consistent with the short-lifetime component observed for RB in water.

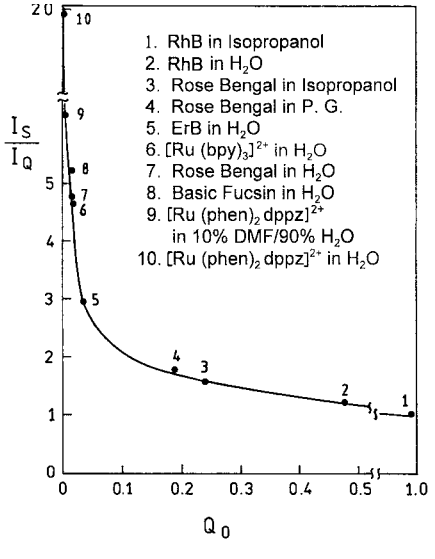

FIG. 15. Enhancement of the emission of fluorophores with different quantum yields.

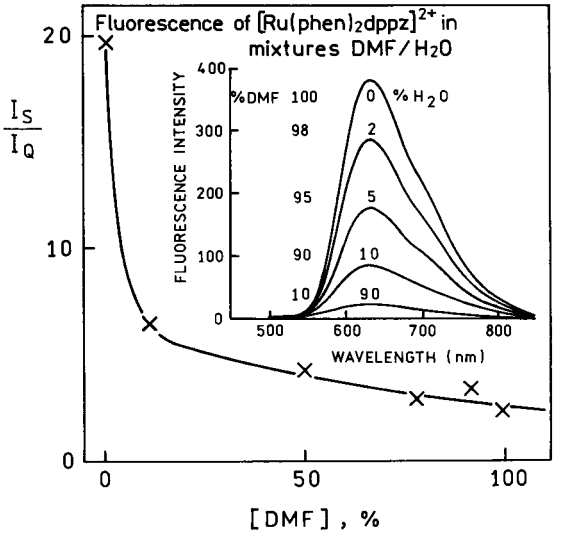

FIG. 16. Enhancement of $[Ru(bpy)_2(dppz)]^{2+}$ on silver island films in water–DMF mixtures.

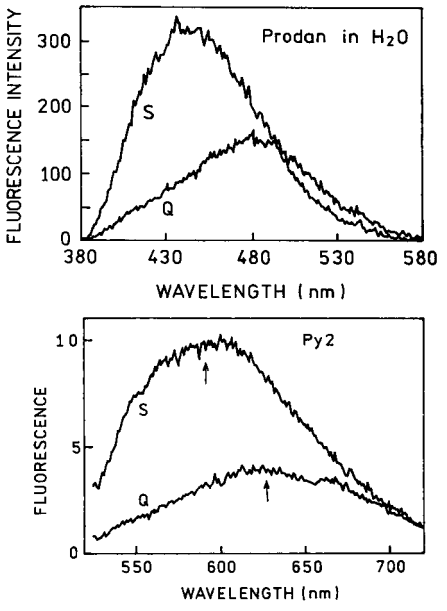

FIG. 17. Effects of silver island films on solvent-sensitive fluorophores.

For instance, a value of G_F for RB predicts a lifetime of 35 ps. Additional studies are needed to clarify the range of G_F and G_A values that result from fluorophore–metal interaction.

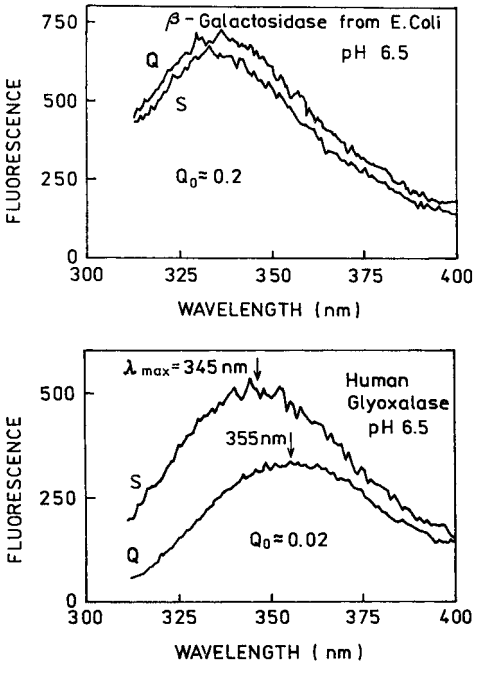

FIG. 18. Emission spectra of a higher-quantum-yield protein β-galactosidase from *E. coli* (0.05 mg/ml) and a lower-quantum-yield protein human glyoxalase (0.15 mg/ml) between quartz plates (Q) and silver island films (S). The excitation wavelength was 295 nm.

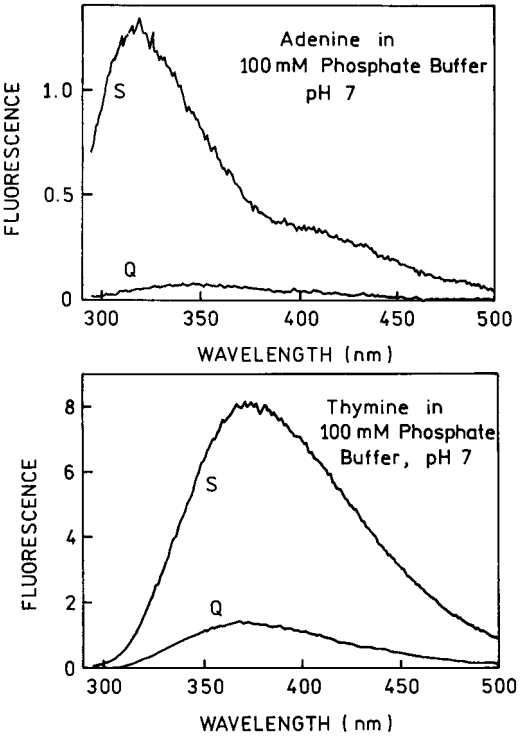

FIG. 19. Effects of silver island films on nucleic acid bases. The concentrations of adenine and thymine were 1.2 and 1.3 mM, respectively, in 100 mM phosphate buffer, pH 7.

Spectral Shifts in the Presence of Silver Islands

In our recent publication we predicted that solvent-sensitive fluorophores near silver islands would display emission shifts to shorter wavelengths (16). It is known that the extent of solvent or spectral relaxation depends on both the fluorescence lifetime (τ) and the solvent relaxation time (τ_R). This dependence is given by

$$\bar{\nu}_{cg} = \bar{\nu}_\infty + (\bar{\nu}_0 - \bar{\nu}_\infty)\frac{\tau_R}{\tau + \tau_R}, \qquad [12]$$

where $\bar{\nu}_{cg}$ is the emission center of gravity, and ν_0 and ν_∞ are the initially excited and fully relaxed states, respectively (36).

Figure 17 shows the emission spectra of two solvent-sensitive fluorophores between quartz plates and silver islands. In both cases we observed blue shifts in the emission, which are consistent with a decreased lifetime of fluorophores near the islands (Eq. [12]). Since fluorophores within 50 Å of the metal are likely to be quenched, it is unlikely that the blue shifts seen in Fig. 17 are due to fluorophores bound to the silver islands. Binding of fluorophores to the uncoated quartz surface is also unlikely to be the cause of the spectral shifts

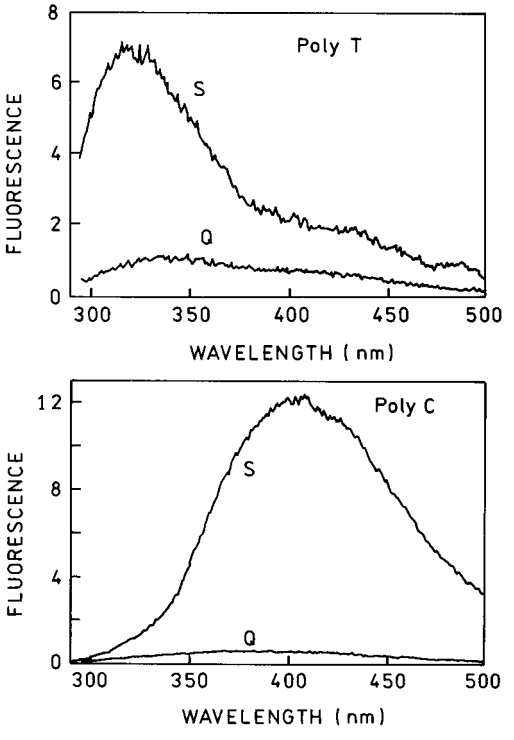

FIG. 20. Effect of silver island films on single-stranded poly(T) (top) and poly(C) (bottom). The concentrations of poly(T) (15-mer) and poly(C) (15-mer) were 10 mM in 100 mM phosphate buffer, pH 7. The excitation wavelength was 285 nm.

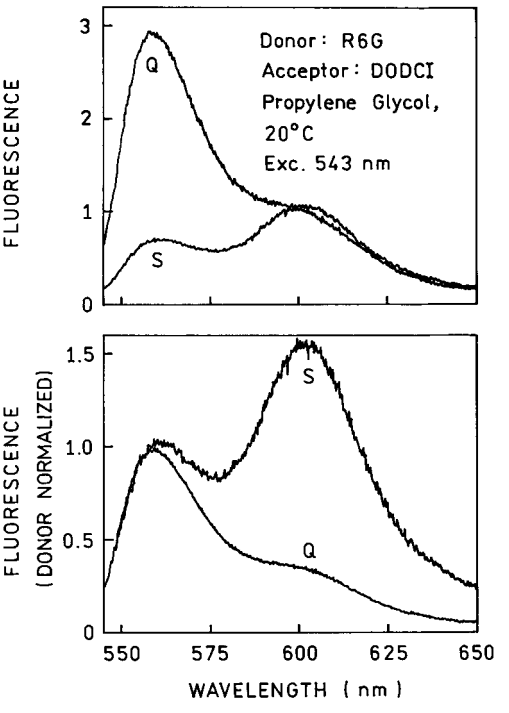

FIG. 21. Emission of mixture rhodamine 6G (donor) and DODCI (acceptor) on quartz (Q) and silver island film (S). The emission spectra in the lower panel are normalized to the donor emission. The R6G donor and DODCI acceptor concentrations were 4×10^{-4} and 4×10^{-4} M, respectively. By analogy with similar fluorophores the Forster distance (R_0) exceeds 55 Å.

since uncoated quartz is present for both emission spectra.

Effects of Silver Islands on Intrinsic Protein Fluorescence

We examined the emission spectra of two proteins in the presence and absence of silver islands (Fig. 18). The proteins β-galactosidase and glyoxalase were selected for their modest and low quantum yields. The quantum yield of *E. coli* β-galactosidase was found to be 0.18 relative to that of *N*-acetyl-L-tryptophamide (NATA) (37) which is reported to be 0.13 (38). The quantum yield of human glyoxalase was found to be about 10-fold less and, thus, near 0.013. β-Galactosidase is a tetrameric protein, 480,000 molecular weight, which contains 26 tryptophan residues in each 120,000-Da subunit (39). Human glyoxalase is a 66,000-Da monomer that contains two tryptophan residues (40). For the higher-quantum-yield β-galactosidase there was no significant effect of the silver islands on the emission spectra. For the lower-quantum-yield human glyoxalase we observed both a blue shift and an increase in emission intensity. We attribute the spectral changes in Fig. 18 (bottom) as due to increased emission from a highly quenched tryptophan residue in glyoxyalase. Because the enhanced emission spectrum is blue shifted we conclude the low-quantum-yield tryptophan residue is shielded from the solvent. The absence of a spectral shift or enhancement in β-galactosidase is understandable given its large number of tryptophan residues since it is unlikely that a significant fraction of these are highly quenched. These re-

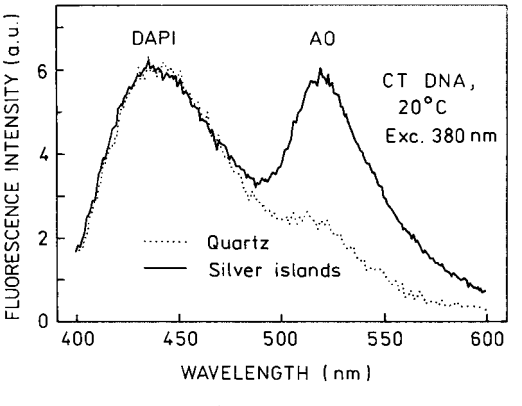

FIG. 22. Emission spectra of DNA labeled with DAPI (donor) and acridine orange (acceptor) between quartz plates and silver island films. The spectra are normalized to the donor emission. The concentration of DNA in 100 mM phosphate buffer, pH 7, was 2 mM as base pairs. The concentration of DAPI and acridine orange were 1 per 100 bp and 1 per 7000 bp, respectively.

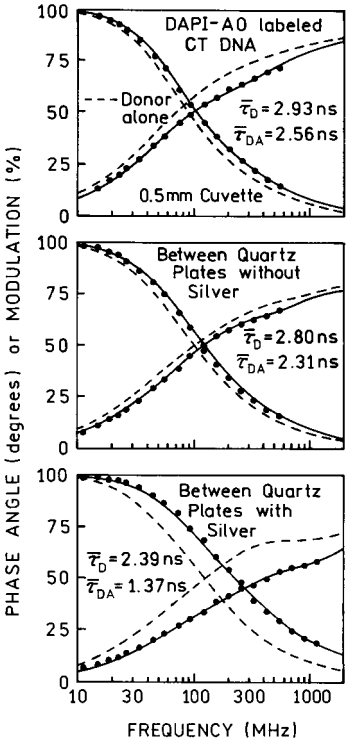

FIG. 23. Frequency-domain DAPI donor decays when bound to DNA.

sults suggest that silver islands can result in increased emission from quenched aromatic amino acid residues in proteins. Further work is required to determine if the protein structures are perturbed by contact with the silver islands.

Effects of Silver Islands on Nucleic Acid Bases and DNA

The intrinsic emission from DNA, nucleotides, and nucleic acid bases is very weak (41–43) and is difficult to observe even with modern instrumentation (45, 46). We questioned whether silver islands could enhance this weak intrinsic fluorescence. Emission spectra of the bases adenine and thymine are shown in Fig. 19. These spectra show increased emission from these bases occurs in the presence of the silver islands. Similar results were obtained for the single-stranded oligonucleotides poly(T) and poly(C) (Fig. 20). The long-wavelength emission maximum of poly(C) is in agreement with that reported previously (45). Additionally, we have observed enhanced emission from double-helical DNA near silver islands and the increased emission was accompanied by a decreased lifetime (46). These results could be of importance for the growing use of DNA arrays or gene chips (47–49) or attempts to sequence DNA using a single strand of DNA (50–52).

Effects of Silver Islands on Resonance Energy Transfer

Resonance energy transfer is widely used in biochemical (53–55) and biomedical research (56, 57). RET occurs whenever fluorophores with suitable spectral properties come within the Forster distance R_0. Forster distances range from 20 to 40 Å, and are rarely larger than 50 Å. Theoretical studies of donors and acceptors at appropriate locations near metal particles have been predicted to increase the rates of energy transfer by a factor of 100-fold or larger at distances as long as 700 Å (7, 8). To the best of our knowledge there have been no experimental demonstrations of increased energy transfer near metal surfaces.

We examined the effects of silver island films on RET between the donor rhodamine 6G (R6G) and acceptor DODCI when dissolved in a homogeneous solution. Emission spectra of this mixture are shown in Fig. 21. The presence of silver islands results in a dramatic drop in the donor intensity (top panel). The lower panel of Fig. 21 shows the emission spectra normalized to the donor emission. In this case the dramatic increase in acceptor emission becomes more apparent. Since we have already shown that the islands have no effect on rhodamine B under our conditions (Fig. 4, above), the intensity decrease seen in Fig. 19 is attributed to increased energy transfer to DODCI. This interpretation is supported by the increase in acceptor emission.

TABLE 4

Photophysical Parameters of $[Ru(bpy)_2(dppz)]^{2+}$ in Water–Dimethylformamide (DMF) Mixtures

% DMF (v/v)	Q^a	Q_m/Q	τ (ns)	k_{nr} (ns^{-1})	Γ (ns^{-1})	I_S/I_Q (obs)	I_S/I_Q (calc)[b]
100	0.0112	2.2	139.4	0.0071	8×10^{-5}	2.0	2.57
98	0.0085	2.9	113.4	0.0087	7.5×10^{-5}	2.9	2.92
95	0.0054	3.4	80.2	0.0124	6.7×10^{-5}	3.4	3.56
90	0.0027	4.3	42.2	0.0236	6.4×10^{-5}	4.3	4.60
10	0.008	6.4	12.9	0.0775	6.2×10^{-5}	6.4	6.04

[a] The quantum yields are measured relative to $[Ru(bpy)_3]^{2+}$ in air-equilibrated water with an assumed quantum yield of 0.02.
[b] Calculated using Eq. [A7] with $G_F = 254$, $G_A = 16$, $d_m = 8$ Å, and $d_q = 40$ Å fixed.

TABLE 5

Multiexponential Analysis of the DAPI Donor Intensity Decay in the Absence and Presence of Acceptor and Silver Islands

Sample	$\bar{\tau}$ (ns)[a]	α_1	τ_1 (ns)	α_2	τ_2 (ns)	α_3	τ_3 (ns)	χ^2_R
DAPI-DNA, C	2.93	0.278	0.63	0.722	3.11	—	—	2.1
DAPI-DNA, Q	2.80	0.311	0.16	0.391	1.15	0.298	3.62	2.2
DAPI-DNA, S	2.39	0.447	0.09	0.414	1.29	0.139	3.70	2.1
DAPI-AO-DNA, C	2.56	0.497	0.50	0.503	2.91	—	—	3.5
DAPI-AO-DNA, Q	2.31	0.449	0.24	0.419	1.64	0.132	3.71	2.4
DAPI-AO-DNA, S	1.37	0.599	0.09	0.293	0.59	0.108	2.22	4.0

[a] $\bar{\tau} = \Sigma_i f_i\tau_2$, $f_i = \alpha_i f_i/\Sigma f_i\tau_i$.

As a final experiment we examined resonance energy transfers from DAPI to acridine orange (AO) when bound to double-helical calf thymus DNA (Fig. 22). In this case the bulk concentrations of the donor and acceptor are lower because they are held in close proximity by the DNA. There is a dramatic increase in the acceptor emission near 520 nm which we believe is due to a metal-enhanced increase in the extent of energy transfer. This interpretation is supported by the frequency-domain intensity decays of the DAPI donor (Fig. 23). The mean decay time of the donor alone ($\bar{\tau}_D$) decreases from 2.80 ns between the quartz plates to 2.39 ns between the silver islands (Table 5). In contrast, for DAPI in the presence of acceptor the mean decay time ($\bar{\tau}_{DA}$) decreases nearly twofold, from 2.31 to 1.37 ns between quartz and silver islands, respectively. These results indicate a significant increase in energy transfer near the silver islands.

DISCUSSION

The results described above represent the first step in using metallic surface-enhanced fluorescence for biochemical research. The results are qualitative because only a small fraction of the sample volume is within the volume affected by the silver islands. Nonetheless, the results demonstrate that metallic surfaces can result in substantial changes in the spectral properties of biochemical fluorophores and, importantly, increased quantum yields from weakly fluorescent molecules. One can imagine numerous opportunities when using these effects of metallic surfaces, including detection of DNA based on its intrinsic fluorescence, observation of weakly fluorescent residues in proteins, detection of membranes adjacent to metal surfaces based on spectral shifts of polarity-sensitive fluorophores, and detection of binding events using weakly fluorescent probes which become localized near the metal surfaces. Additionally, the metal-induced increase in energy transfer may allow immunoassays and DNA hybridization measurements with widely spaced donors and acceptors.

APPENDIX

Model for Fluorescence Intensities and Intensity Decays for Samples between Silver Island Films

The samples used in this article are spatially heterogeneous with an overall thickness d (Scheme 1). The sample contains a dominant volume distant from the SIFs which we call the bulk volume. There is a region of thickness d_q immediately adjacent to the SIFs where the emission is quenched. At distance d_q from the quartz plates there is a region of thickness d_m where the emission is enhanced by the metal. This geometric model is used to simplify the actual situation where both the quenching and enhancement interactions depend on distance. In the bulk solution the quantum yields and lifetimes are given by

$$Q_0 = \frac{\Gamma}{\Gamma + k_{nr}}, \qquad [A1]$$

$$\tau_0 = \frac{1}{\Gamma + k_{nr}}. \qquad [A2]$$

In our experiments we examined the intensity using front face excitation. In the absence of SIFs between the quartz plate the intensity is given by

$$I_Q = I_0 d C \epsilon_0 Q_0, \qquad [A3]$$

where I_0 is the incident intensity, c is the concentration, and ϵ_0 is the extinction coefficient. The fluorescence intensity from the sample between SIFs is more complex. The metal increases the emission rate to $G_F\Gamma$. We can imagine two limiting cases: one where the metal affects the fluorescence emission, and a second where the metal also affects the amount of light absorbed or, equivalently, the extinction coefficient. This effect is represented by an effective extinction coefficient $\epsilon_m = G_A\epsilon_0$ in the enhancement region where G_A is the factor increase in light absorption. If the effects of the metal are the same for absorption and emission then $G_A = G_F = G$. If the effects are not equivalent

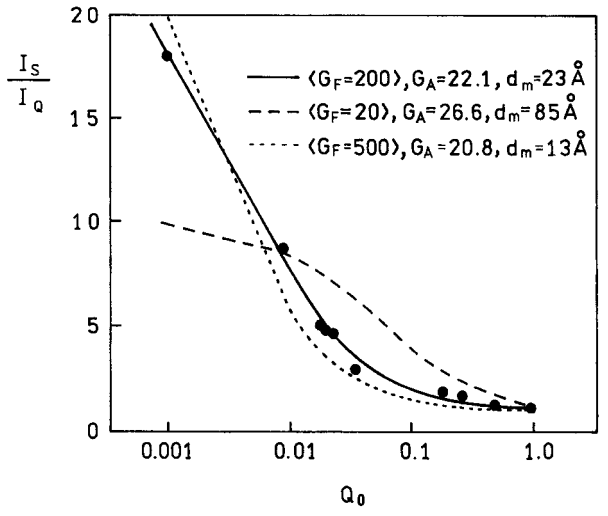

FIG. A1. Comparison of Eq. [A5] with the enhancements reported in Fig. 15. The values in angle brackets were held fixed at the indicated values during the fitting procedure.

than $G_A \neq G_F$. And if the metal affects only the emission than $G_A = 1.0$. In the quenching region we assume the extinction coefficient in $\epsilon_q = G_q\epsilon_0$ and the quantum yield is Q_q. Our samples are optically thin so we need not consider inner filter effects. The fluorescence intensity between the SIFs is given by

$$I_S = I_0 c\epsilon_0[(d - 2(d_n + d_q))Q_0 + 2G_A d_m Q_m + 2G_A G_q d_q Q_q]. \quad [A4]$$

For simplicity we assume $Q_q = 0$. The ratio of the fluorescence intensity in the presence and absence of the SIFs is given by

$$\frac{I_S}{I_Q} = \frac{d - 2(d_m + d_q)}{d} + \frac{2G_A d_m}{d}\frac{G_F(\Gamma + k_{nr})}{G_F\Gamma + k_{nr}}. \quad [A5]$$

We used this expression (Eq. [A5]) to predict the effects of SIFs on fluorophores with various quantum yields, for various values of the assumed parameters (Fig. A1). These simulations show that the enhancement seen for various-quantum-yield fluorophores (Fig. 15) are consistent with a 200-fold increase in the radiative rate ($G_F = 200$) and a 22-fold increase in absorption ($G_A = 22$) near the metal. However, the recovered distance of 23 Å seems too small when compared with theoretical predictions. Further studies are needed to further clarify the values of G_A, G_F, and d_m.

ACKNOWLEDGMENTS

This work was supported by the NIH National Center for Research Resources, RR-08119, with additional support from the Juvenile Diabetes Foundation International, 1-2000-546, and the American Diabetes Foundation. The authors thank the referees for the detailed comments and suggestions which improved the manuscript.

REFERENCES

1. Ford, G. W., and Weber, W. H. (1984) Electromagnetic interactions of molecules with metal surfaces. *Phys. Rep.* **113,** 195–287.
2. Chance, R. R., Prock, A., and Silbey, R. (1978) Molecular fluorescence and energy transfer near interfaces. *Adv. Chem. Phys.* **37,** 1–65.
3. Barnes, W. L. (1998) Fluorescence near interfaces: The role of photonic mode density. *J. Mod. Opt.* **45,** 661–699.
4. Gersten, J. I., and Nitzan, A. (1985) Photophysics and photochemistry near surfaces and small particles. *Surf. Sci.* **158,** 165–189.
5. Kummerlen, J., Leitner, A., Brunner, H., Aussenegg, F. R., and Wokaun, A. (1993) Enhanced dye fluorescence over silver island films: Analysis of the distance dependence. *Mol. Phys.* **80,** 1031–1046.
6. Drexhage, K. H. (1974) Interaction of light with monomolecular dye layers, in Progress in Optics (Wolf, E., Ed.), pp. 163–232, North–Holland, Amsterdam.
7. Gersten, J. I., and Nitzan, A. (1984) Accelerated energy transfer between molecules near a solid particle. *Chem. Phys. Lett.* **104,** 31–37.
8. Hua, X. M., Gersten, J. I., and Nitzan, A. (1985) Theory of energy transfer between molecules near solid state particles. *J. Chem. Phys.* **83,** 3650–3659.
9. Strickler, S. J., and Berg, R. A. (1962) Relationship between absorption intensity and fluorescence lifetimes of molecules. *J. Chem. Phys.* **37,** 814–822.
10. Selvan, S. T., Hayakawa, T., and Nogami, M. (1999) Remarkable influence of silver islands on the enhancement of fluorescence from Eu^{3+} ion-doped silica gels. *J. Phys. Chem. B* **103,** 7064–7067.
11. Leitner, A., Lippitsch, M. E., Draxler, S., Riegler, M., and Aussenegg, F. R. (1985) Fluorescence properties of dyes absorbed to silver islands, investigated by picosecond techniques. *Appl. Phys. B* **36,** 105–109.
12. Wokaun, A., Lutz, H.-P., King, A. P., Wild, U. P., and Ernst, R. R. (1983) Energy transfer in surface enhanced fluorescence. *J. Chem. Phys.* **79,** 509–514.
13. Link, S., and El-Sayed, M. A. (1999) Spectral properties and relaxation dynamics of surface plasmon electronic oscillations in gold and silver nanodots and nanorods. *J. Phys. Chem. B* **103,** 8410–8426.
14. Link, S., and El-Sayed, M. A. (2000) Shape and size dependence of radiative, nonradiative and photothermal properties of gold nanocrystals. *Int. Rev. Phys. Chem.* **19,** 409–453.
15. Kreibig, U., Vollmer, M., and Toennies, J. P. (1995) Optical Properties of Metal Clusters, Springer-Verlag, Berlin.
16. Lakowicz, J. R. (2001) Radiative decay engineering. *Anal. Biochem.* **298,** 1–24.
17. Gersten, J., and Nitzan, A. (1981) Spectroscopic properties of molecules interacting with small dielectric particles. *J. Chem. Phys.* **75,** 1139–1152.
18. Creighton, D. J., and Hamilton, D. S. (2001) Brief history of glyoxalase I and what we have learned about metal ion dependent enzyme catalyzed isomerizations. *Arch. Biochem. Biophys.* **387,** 1–10.
19. Nucci, A. R., Moracci, M., Vacarro, C., Vespa, N., and Rossi, M. (1993) Exoglucosidase activity and substrate specificity of the β-glycosidase from the extreme thermophilic *Sulfolobus solfataricus*. *Biotechnol. Appl. Biochem.* **17,** 239–250.

20. D'Auria, S., unpublished results.
21. Laczko, G., Gryczynski, I., Gryczynski, Z., Wiczk, W., Malak, H., and Lakowicz, J. R. (1990) A 10-GHz frequency-domain fluorometer. *Rev. Sci. Instrum.* **61,** 2331–2337.
22. Lakowicz, J. R., Laczko, G., Cherek, H., Gratton, E., and Limkeman, M. (1994) Analysis of fluorescence decay kinetics from variable-frequency phase shift and modulation data. *Biophys. J.* **46,** 463–477.
23. Kerker, M. (1985) The optics of colloidal silver: Something old and something new. *J. Colloid Interface Sci.* **105,** 297–314.
24. Mulvaney, P. (1996) Surface plasmon spectroscopy of nanosized metal particles. *Langmuir* **12,** 788–800.
25. Rivas, L., S.-C., S., Garcia-Ramos, J. V., and Morcillo, G. (2001) Growth of silver colloidal particles obtained by citrate reduction to increase the raman enhancement factor. *Langmuir* **17,** 574–577.
26. Jensen, T. R., Malinsky, M., Duval, H., Christy, L., and Van Duyne, R. P. (2000) Nanosphere lithography: Tunable localized surface plasmon resonance spectra of silver nanoparticles. *J. Phys. Chem. B* **104,** 10549–10556.
27. Singer, R. R., Leitner, A., and Aussenegg, F. R. (1995) Structure analysis and models for optical constants of discontinuous metallic silver films. *J. Opt. Soc. Am. B* **12,** 220–228.
28. Soper, S. A., Nutter, H. L., Keller, R. A., Davis, L. M., and Shera, E. B. (1993) The photophysical constants of several fluorescent dyes pertaining to ultrasensitive fluorescence spectroscopy. *Photochem. Photobiol.* **57,** 972–977.
29. Van Orden, A., Machara, N. P., Goodwin, P. M., and Keller, R. A. (1998) Single-molecule identification in flowing sample streams by fluorescence burst size and intraburst fluorescence decay rate. *Anal. Chem.* **70,** 1444–1451.
30. Ambrose, W. P., Goodwin, P. M., Jett, J. H., Van Orden, A., Wemer, J. H., and Keller, R. A. (1999) Single molecule fluorescence spectroscopy at ambient temperature. *Chem. Rev.* **99,** 2929–2956.
31. Jovin, T. M., and Arndt-Jovin, D. J. (1989) FRET microscopy: Digital imaging of fluorescence resonance energy transfer. Application in cell biology, *in* Cell Structure and Function by Microspectrofluorometry (Kohen, E., Hirschberg, J. G., and Ploem, J. S., Eds.), pp. 99–117, Academic Press, London.
32. Van Houten, J., and Watts, R. J. (1975) The effect of ligand and solvent deuteration on the excited state properties of the tris(2,2′-bipyridyl)ruthenium(II) ion in water. Evidence for electron transfer to solvent. *J. Am. Chem. Soc.* **97,** 3843–3844.
33. Harriman, A. (1977) Photochemistry of a surfactant derivative of tris(2,2′-bipyridyl)ruthenium(II). *J. Chem. Soc. Chem. Commun.*, 777–778.
34. Nair, R. B., Cullum, B. M., and Murphy, C. J. (1997) Optical properties of $[Ru(phen)_2dppz]^{2+}$ as a function of nonaqueous environment. *Inorg. Chem.* **36,** 962–965.
35. Turro, C., Bossmann, S. H., Jenkins, Y., Barton, J. K., and Turro, N. J. (1995) Proton transfer quenching of the MLCT excited state of $Ru(phen)_2dppz^{2+}$ in homogeneous solution and bound to DNA. *J. Am. Chem. Soc.* **117,** 9026–9032.
36. Lakowicz, J. R. (1999) Principles of Fluorescence Spectroscopy, Kluwer Academic/Plenum, New York.
37. D'Auria, S., DiCesare, N., Gryczynski, I., Rossi, M., and Lakowicz, J. R. (2001) On the effect of SDS on the structure of β-galactosidase from *E. coli. J. Biochem.*, in press.
38. Demchenko, A. P. (1981) Ultraviolet Spectroscopy of Proteins, Springer-Verlag, New York.
39. Jacobson, R. H., Zhang, X. J., DuBose, R. F., and Matthews, B. W. (1994) Three-dimensional structure of β-galactosidase from *E. coli. Nature* **369,** 761–766.
40. D'Auria, S., unpublished results.
41. Daniels, M., and Hauswirth, W. (1971) Fluorescence of the purine and pyrimidine bases of the nucleic acids in neutral aqueous solution at 300 K. *Science* **171,** 675–677.
42. Ballini, J. P., Vigny, P., and Daniels, M. (1983) Synchrotron excitation of DNA fluorescence decay time evidence for excimer emission at room temperature. *Biophys. Chem.* **18,** 61–65.
43. Georghiou, S., Nordlund, Thomas M., and Saim, A. M. (1985) Picosecond fluorescence decay time measurements of nucleic acids at room temperature in aqueous solution. *Photochem. Photobiol.* **41,** 209–212.
44. Georghiou, S., Braddick, T. D., Philippetis, A., and Beechem, J. M. (1996) Large-amplitude picosecond anisotropy decay of the intrinsic fluorescence of double-stranded DNA. *Biophys. J.* **70,** 1909–1922.
45. Plessow, R., Brockhinke, A., Eimer, W., and Kohse-Hoinghaus, Katharina (2000) Intrinsic time- and wavelength-resolved fluorescence of oligonucleotides: A systematic investigation using a novel picosecond laser approach. *J. Phys. Chem. B* **104,** 3695–3704.
46. Lakowicz, J. R., Shen, Y., Gryczynski, Z., D'Auria, S., and Gryczynski, I. (2001) Intrinsic fluorescence from DNA can be enhanced by metallic particles. *Biochem. Biophys. Res. Comm.* **286,** 875–879.
47. Lipshutz, R. J., Fodor, Stephen, P. A., Gingeras, Thomas, R., and Lockhart, David J. (1999) High density synthetic oligonucleotide arrays. *Nat. Genet. Suppl.* **21,** 20–24.
48. Hacia, J. G., and Collins, F. S. (1999) Mutational analysis using oligonucleotide microarrays. *J. Med. Genet.* **36,** 730–736.
49. Ferea, T. L., and Brown, P. O. (1999) Observing the living genome. *Curr. Opin. Genet. Dev.* **9,** 715–722.
50. Knemeyer, J-P., Marme, N., and Sauer, M. (2000) Probes for detection of specific DNA sequences at the single-molecule level. *Anal. Chem.* **72,** 3717–3724.
51. Enderlein, J., Robbins, D. L., Ambrose, W. P., and Keller, R. A. (1998) Molecular shot noise, burst size distribution, and single-molecule detection in fluid flow: Effects of multiple occupancy. *J. Phys. Chem.* **102,** 6089–6094.
52. Van Orden, A., Machara, N. P., Goodwin, P. M., and Keller, R. A. (1998) Single-molecule identification in flowing sample streams by fluorescence burst size and intraburst fluorescence decay rate. *Anal. Chem.* **70,** 1444–1451.
53. Cheung, H. C. (1991) Resonance energy transfer, *in* Topics in Fluorescence Spectroscopy, Vol. 2: Principles (Lakowicz, J. R., Ed.), pp. 127–176, Plenum, New York.
54. Wu, P., and Brand, L. (1994) Review: Resonance energy transfer methods and applications. *Anal. Biochem.* **218,** 1–13.
55. Miyawaki, A., Llopis, J., Heim, R., McCaffery, J. M., Adams, J. A., Ikura, M., and Tsien, R. Y. (1997) Fluorescent indicators for Ca^{2+} based on green fluorescent proteins and calmodulin. *Nature* **388,** 882–887.
56. Morrison, L. E., and Stols, L. M. (1993) Sensitive fluorescence based thermodynamic and kinetic measurements of DNA hybridization in solution. *Biochemistry* **32,** 3095–3104.
57. Ju, J., Glazer, A. N., and Mathies, R. A. (1996) Energy transfer primers: A new fluorescence labeling paradigm for DNA sequencing and analysis. *Nat. Med.* **292,** 246–249.